

Time resolved reflectivity measurements of convective clouds

Brenda Dolan¹, Pavlos Kollias², Susan C van den Heever¹, Kristen Rasmussen¹, Mariko Oue², Edward P. Luke³, Katia Lamer⁴, Bernat P Treserras⁵, Ziad S Haddad⁶, Graeme Stephens⁷, and V Chandrasekar⁸

¹Colorado State University

²Stony Brook University

³Brookhaven National Laboratory (DOE)

⁴Brookhaven National Laboratory

⁵McGill University

⁶Jet Propulsion Lab (NASA)

⁷JPL/Caltech

⁸Department of Electrical and Computer Engineering, Colorado State University, Fort Collins, CO 80523, USA

August 12, 2023

Abstract

NASA's Investigations of Convective Updrafts (INCUS) mission aims to document convective updraft mass flux through changes in the radar reflectivity (ΔZ) in convective cores captured by a constellation of three Ka-band radars sampling the same convective cells over intervals of 30, 90 and 120 s. Here, high spatiotemporal resolution observations of convective cores from surface-based radars that use agile sampling techniques are used to evaluate aspects of the INCUS measurement approach using real observations. Analysis of several convective cells confirms that large coherent ΔZ structure with measurable signal (> 5 dB) can occur in less than 30 s and are correlated with underlying convective motions. The analysis indicates that the INCUS mission radar footprint and along track sampling are adequate to capture most of the desirable ΔZ signals. This unique demonstration of reflectivity time-lapse provides the framework for estimating convective mass flux independent from Doppler techniques with future radar observations.

Hosted file

970174_0_art_file_11237601_ryjlf8.docx available at <https://authorea.com/users/650746/articles/659090-time-resolved-reflectivity-measurements-of-convective-clouds>

1
2 Time resolved reflectivity measurements of convective clouds
3
4
5
6

7 Brenda Dolan¹, Pavlos Kollias^{2,3}, Susan C. van den Heever¹, Kristen L.
8 Rasmussen¹, Mariko Oue², Edward Luke³, Katia Lamer³, Bernat P. Treserras⁴,
9 Ziad Haddad⁵, Graeme Stephens⁵, and V. Chandrasekar¹

10
11
12 ¹Colorado State University, Fort Collins, CO

13 ²School of Marine and Atmospheric Sciences, Stony Brook University,
14 Stony Brook, NY

15 ³Brookhaven National Laboratory, Upton, New York

16 ⁴McGill University, Montreal, Quebec, Canada

17 ⁵Jet Propulsion Laboratory, California Institute of Technology, Pasadena CA
18
19

20 Manuscript for *Geophysical Research Letters*
21
22

23 **Key Points**
24

25 Convective motions can cause measurable ΔZ changes in time intervals as short as 30 sec.
26

27 The reflectivity time-lapse rate technique relates to spatially and temporally coherent structures
28 and the underlying convective motions.
29

30 The INCUS mission radar sampling characteristics are adequate for capturing most of the ΔZ
31 changes caused by convective motions.
32

33 **Abstract**

34

35 NASA's Investigations of Convective Updrafts (INCUS) mission aims to document convective
36 updraft mass flux through changes in the radar reflectivity (ΔZ) in convective cores captured by
37 a constellation of three Ka-band radars sampling the same convective cells over intervals of 30,
38 90 and 120 s. Here, high spatiotemporal resolution observations of convective cores from
39 surface-based radars that use agile sampling techniques are used to evaluate aspects of the
40 INCUS measurement approach using real observations. Analysis of several convective cells
41 confirms that large coherent ΔZ structure with measurable signal (> 5 dB) can occur in less than
42 30 s and are correlated with underlying convective motions. The analysis indicates that the
43 INCUS mission radar footprint and along track sampling are adequate to capture most of the
44 desirable ΔZ signals. This unique demonstration of reflectivity time-lapse provides the
45 framework for estimating convective mass flux independent from Doppler techniques with future
46 radar observations.

47

48 **Plain Language Summary:**

49 The vertical transport of water between Earth's surface and the upper troposphere afforded by
50 convective storms is a driving factor of weather and climate. However, observing dynamic
51 processes at the scales of convection has been a challenge due to the transient and rapidly
52 evolving nature of convection, as well as sensor and resource limitations. High-resolution time-
53 lapses of radar reflectivity are used to investigate the movement of air and water within deep,
54 intense storms. This is a unique approach to understanding how water and air move throughout
55 the atmosphere in strong storms. It is shown that large changes in reflectivity are apparent even
56 over time scales less than 30 seconds, which are inferred to be due to strong vertical motions. A
57 new NASA satellite mission called INCUS (Investigations of Convective Updrafts) seeks to use
58 the same methods to estimate the movement of air and water globally across the tropics.

59

60 **1. Introduction**

61
62 Convective clouds play a critical role in the Earth's climate system, acting as sinks of total
63 water in the atmospheric column through precipitation, thereby contributing to the atmospheric
64 energy balance and water cycle. They also serve as a primary mechanism for the transport of
65 thermal energy, moisture, and momentum through the troposphere, thereby significantly
66 impacting the large-scale atmospheric circulation and local environment, and affecting the
67 probability of subsequent cloud formation (e.g., Hartmann et al. 1984; Su et al. 2014; Sherwood
68 et al. 2014). Because convective clouds evolve rapidly, their microphysical and kinematic
69 properties and lifecycles are challenging to resolve in models, and even in observations (e.g.,
70 Fridlind et al. 2017; Oue et al., 2019, Marinescu et al. 2020). Noticeably, a knowledge gap on the
71 convective updraft core properties (i.e., intensity, size, depth, lifecycle) and their dependency on
72 environmental factors exists. Such measurements are not only particularly challenging to obtain
73 over the remote tropical oceans but also over land due to the transient and rapidly evolving
74 nature of convection, as well as due to limitations of existing observing systems (e.g., Oue et al.,
75 2019).

76 To methodically advance observation-based understanding of fundamental convective cloud
77 processes, new observational approaches are needed. Emerging new technologies such as rapid
78 scanning or phased-array radars (PARs) have the potential to cope with the rapid transient nature
79 of convection (Bluestein et al., 2010, Pazmany et al. 2013, Tanamachi and Heinselman 2015,
80 Bluestein et al., 2019, Palmer et al. 2022, Kollias et al. 2022b), but robust and detailed
81 measurements of the vertical evolution of convection have not been largely explored. At a
82 minimum, when available, PARs should be able to provide high spatiotemporal resolution
83 observations of convective cores over land (Kollias et al., 2022b). In addition, the explosive
84 growth of CubeSats (Stephens et al., 2020a, Peral et al., 2019) and new planned satellite missions
85 that all feature Doppler velocity measurements have the potential to provide the first global
86 climatology of convective dynamics. For example, the joint European Space Agency (ESA) and
87 Japanese Aerospace Exploration Agency (JAXA) Earth Clouds, Aerosols, Radiation Explorer
88 (EarthCARE) mission (Illingworth, et al. 2015, Wehr et al. 2023) will send the first W-band
89 Doppler cloud profiling radar into space in 2024, with the goal of measuring vertical velocities in
90 the upper part of convective clouds. In addition, National Aeronautics and Space Administration

91 (NASA)'s Atmospheric Observing System (AOS) mission is anticipated to include two Doppler
92 radar systems in two different orbits.

93
94 Of particular interest here is NASA's Earth Venture Mission Investigations of Convective
95 Updrafts (INCUS) that encompasses three narrow-swath Ka-band profiling radar satellites,
96 separated by 30, 90 and 120 s between the first and second, second and third, and first and third
97 satellites, respectively. The INCUS radars will provide three curtain (along track and vertical)
98 views of the radar reflectivity field of the same convective cells (Stephens et al., 2020b; van den
99 Heever, et al. 2023). The INCUS convective mass flux (CMF) measurements are not based on
100 the Doppler principle, but instead on the collection of time lapse measurements of reflectivity of
101 convective cores over very short times (termed "the Δt approach") to measure the mass flux on a
102 global scale across the tropics. Similar Δt concepts have been proposed for constellations of
103 passive microwave radiometers (Brogniez et al., 2022). The INCUS CMF measurement
104 approach is based on the idea that over 30, 90 and 120 s time scales, convective dynamics can
105 have a measurable impact on the convective core radar reflectivity structure. In this case, the
106 time resolved radar reflectivity measurements can be used to retrieve the CMF.

107 Here, for the first time, the feasibility of Δt approach is investigated using real observations
108 from high spatiotemporal vertical radar cross-section of convective cores acquired using the
109 Multisensor Agile Adaptive Sampling (MAAS, Kollias et al., 2020) framework. This framework
110 utilizes a comprehensive dataset in real time to guide ground-based sensors (radars) to track and
111 sample convective cores (Lamer et al., 2023). Using the MAAS framework, a large dataset of
112 high spatiotemporal resolution C-band observations were recently collected (section 2), thus,
113 providing a unique dataset for evaluating the INCUS Δt measurement concept (section 3). A few
114 case studies are used to demonstrate that within the INCUS sampling times (30, 90 and 120 sec),
115 noticeable coherent radar reflectivity changes can be observed. These changes are particularly
116 apparent in the upper levels of convective cells and can be related to underlying convective
117 vertical air motion. In addition, the influence of the observed spatiotemporal variability in
118 convective cells on the INCUS measurement methodology is discussed (section 4).

119

120 **2. Methodology**

121

122 A succession of Cloud, Precipitation, Aerosol, and Air Quality Field Experiments in the
123 Coastal Urban Environment of Houston TX took place in the summer of 2022 (Jensen et al.,
124 2022). In particular, the US Department of Energy (DOE) Atmospheric Radiation Measurement
125 (ARM) Tracking Aerosol Convection interactions Experiment (TRACER) and the National
126 Science Foundation (NSF) Experiment of Sea Breeze Convection, Aerosols, Precipitation, and
127 Environment (ESCAPE) field campaigns targeted the study of isolated convective cells in the
128 area of Houston, TX using novel radar cell tracking techniques. Documentation of the lifecycle
129 of isolated convective cells with high spatiotemporal resolution was one key measurement
130 requirement for both field campaigns. To address this measurement need, the field campaigns
131 employed the MAAS framework (Kollias et al., 2020; Lamer et al., 2023). MAAS used
132 observations from the ground-based National Weather Service Next Generation Weather Radar
133 (NEXRAD) in the Houston-Galveston area (KHGX, Crum et al., 1998), supplemented by
134 observations from the Geostationary Operational Environmental Satellites (GOES-16)
135 Geostationary Lightning Mapper (GLM), and the Advanced Baseline Imager (ABI; Griffith et
136 al., 2017) to provide a real-time description (4D data cubes) of the atmospheric state around the
137 Houston area. These “global” observations were used to identify and nowcast the future location
138 of all convective cells in the Houston area. Using a set of rules, MAAS selected a particular
139 convective cell for tracking and transmitted its current and future coordinates to both the DOE
140 ARM 2nd generation C-band Scanning ARM Precipitation Radar (CSAPR2, Kollias et al., 2020)
141 and the CSU C-band Hydrological Instrument for Volumetric Observation (CHIVO). The
142 CSAPR2 sampling strategy was based on sequences of Plain Position Indicator (PPI, constant
143 elevation) sector scans that cover the horizontal extent of convective cells and Range Height
144 Indicator (RHI, constant azimuth) scans that sampled the convective cells from the surface to
145 their cloud top with high spatial resolution. The CSAPR2 RHIs were repeated approximately
146 every 20 s. The CHIVO sampling strategy included only RHI scans with even higher temporal
147 resolution (10 s). Both radars were sampling the same convective cells from different azimuth
148 angles. The width of the CSAPR2 PPI sector scans and the azimuth of the CSAPR2 and CHIVO
149 RHI scans were based on edge computing of key radar parameters such as the azimuth of the
150 maximum reflectivity, the location of the maximum Vertically Integrated Liquid (VIL),
151 maximum low-level convergence, lightning strikes (Lamer et al., 2023). A detailed description of

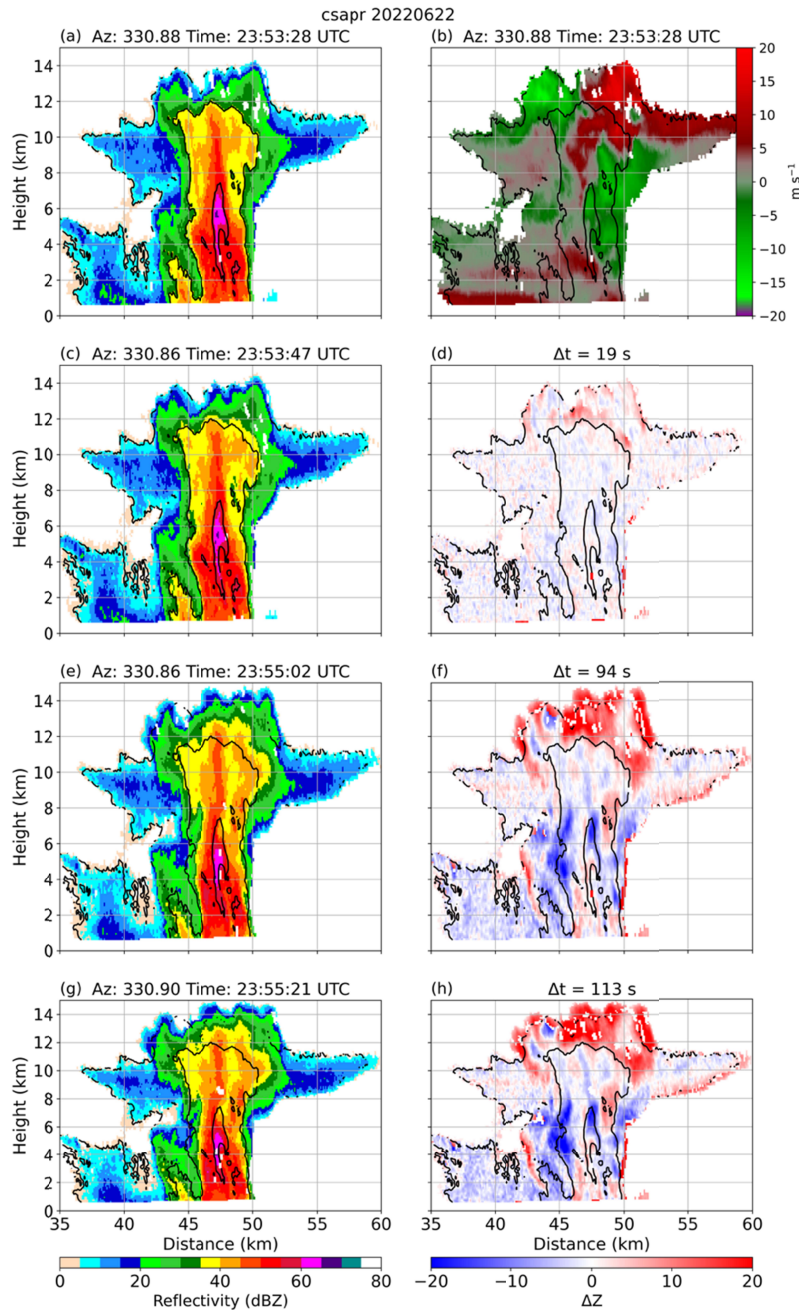
152 the MAAS implementation in the context of the TRACER and ESCAPE field campaigns can be
153 found in Lamer et al. (2023).

154 Here, sequences of RHI scans collected by either CSAPR2 or CHIVO along the same
155 azimuth ($\pm 0.03^\circ$) within 120 s of each other are selected to capture the vertical structure of
156 convective cores as depicted by the radar reflectivity (Z) and its temporal evolution. Oue et al.,
157 (2019; 2022) demonstrated that collecting observations within 2 min reduces the impact of
158 horizontal advection in multi-Doppler wind retrievals. Each RHI is gridded using the Lidar
159 Radar Open Software Environment (LROSE, Bell et al., 2022) Radx2Grid with a grid rotation
160 angle equal to the azimuth of the RHI, essentially reducing the data to a 2-dimensional grid of
161 height and distance from the radar. Storm motion and advection are not specifically accounted
162 for but are both small for the cases presented. To capture the high-resolution aspects of the RHIs,
163 the data were gridded to 100 m in the horizontal (x) and vertical (z) dimension. All reported
164 heights are above ground level (AGL).

165 One of the main objectives of this study is to investigate the impact of the INCUS radar
166 footprint (~ 3 km) on our ability to measure time resolved reflectivity measurements of
167 convective clouds. Thus, the gridded RHI data are also averaged to 3 km horizontal resolution
168 and 250 m vertical resolution to match the horizontal and range resolution of the INCUS
169 spaceborne radars. Using the gridded radar observations, the change in radar reflectivity, herein
170 called ΔZ , is calculated at each grid point by subtracting the reflectivity in dB scale ($\Delta Z = Z_e -$
171 Z_i) between two different radar reflectivity frames collected at two different times ($\Delta t_s = t_e -$
172 t_i), where the subscript i denotes the initial time, e denotes the time of the second RHI, and s is
173 the elapsed time difference between the two radar frames in seconds. In INCUS, three possible
174 ΔZ views of the same convective cells can be measured at Δt increments of $s = 30, 90$ and 120 s
175 that correspond to the ΔZ from the first and second, second and third, and first and third
176 spaceborne radar pairs. A first example of INCUS-like radar observations is depicted in Fig. 1
177 and is generated using a sequence of four CSAPR2 RHI with Δt_e increments of $e = 19, 94,$ and
178 113 s relative to the first RHI. This is the so-called Δt approach proposed to be used by INCUS
179 (van den Heever, 2021).

180

181

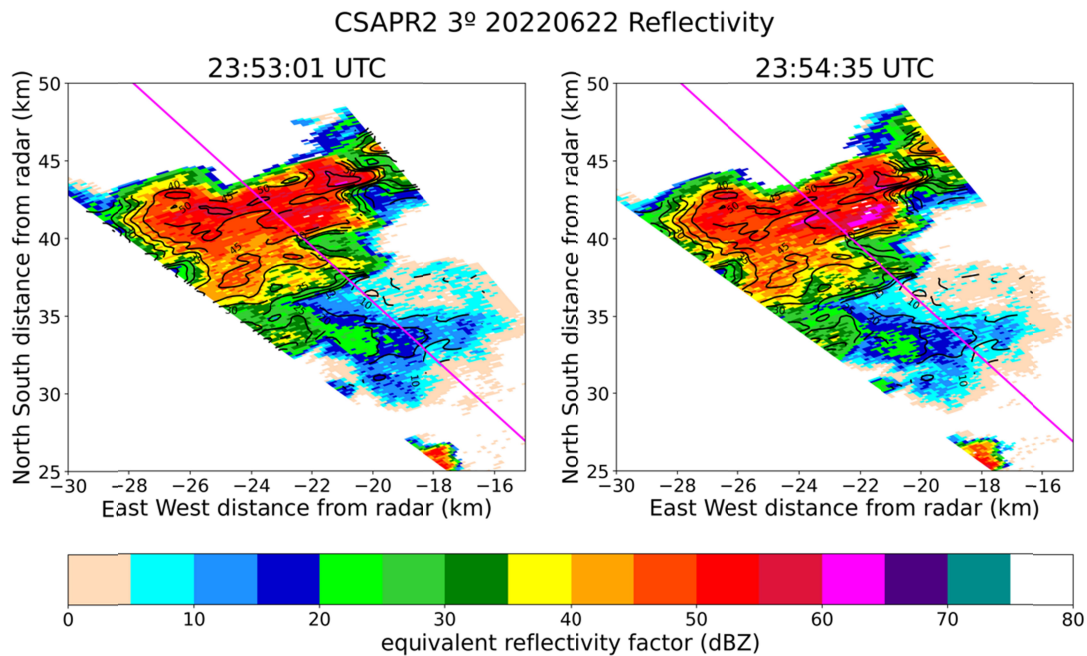


183 Fig. 1: Case 1 demonstration of convective evolution of intense isolated deep convection.
 184 CSAPR2 RHIS at an azimuth of $\sim 330^\circ$ on 22 June 2022 at 23:53:28 UTC, and $\Delta t = 19, 94,$
 185 and
 186 113 s. Black contours represent the 5-, 35-, and 55-dBZ contours at 23:53:28. For reference the
 187 associated radial velocity at t_0 is shown in (b).
 188

189 **3. Results**

191 **a. Case 1: Assessment of convective storm evolution from an intense deep convective**
192 **core**

193
194 The first case study is a convective core targeted by MAAS with the CSAPR2 radar at
195 23:53:28 UTC on 22 June 2022 (Fig. 1). It is an isolated deep convective cell, fairly
196 representative of the types of afternoon convection often observed in the diurnal cycle in the
197 Houston area (Lamer et al., 2023, Oue et al., 2022). The well-developed convective cells exhibit
198 a maximum radar reflectivity of more than 65 dBZ and echo top heights that reach 15 km (Fig.
199 1). In addition to the series of CSAPR2 RHIs that provide high spatiotemporal resolution view of
200 the convective core vertical structure, two consecutive CSAPR2 PPIs at 3° elevation at 23:53:17
201 UTC and 23:54:52 UTC (Δt_{95}) are used to provide the horizontal extent of this isolated
202 convective core (Fig. 2). Despite its intensity and vertical extent, the convective core was less
203 than 10 km wide (Fig. 2). Although some increases in reflectivity at 3.0° elevation are noted over
204 the 95 s (Fig. 2), the overall storm complex has not advected horizontally during the span of the
205 RHIs conducted (Fig. 1).



206
207 Fig. 2: CSAPR2 consecutive PPI sectors (spaced by ~ 90 sec) of Case 1 at 3° in elevation at
208 23:53:01 UTC (left) and 23:54:35 UTC (right). The black contours are the reflectivity from the
209 initial time (23:53:01 UTC) at 5 dB increments. The magenta line represents the CSAPR
210 azimuth of 330.86° corresponding to the RHIs shown in Fig. 1.

211 At $t_0 = 23:53:28$ UTC (Fig. 1a), the C-band radar reflectivity in the convective core exceeded
212 60 dBZ at around 6 km AGL, and the 35 dBZ (0 dBZ) echo top height was 12 km (14.2 km). At
213 Δt_{19} , the ΔZ field indicates an increase in radar reflectivity above 10 km height on the order of +5
214 dB (0.3 dB s^{-1}), while the rest of the echo changes were very close to 0 dB (Fig. 1c, d). The 35
215 dBZ (0 dBZ) echo top height increased by 100 m (300 m) to 12.1 km (14.5 km). While these
216 changes in reflectivity and height are relatively small, they highlight the rapid evolution of
217 convection through changes in reflectivity at very short time scales (19 s), even in non-severe
218 deep convection. A plausible explanation for the increase in the radar reflectivity in the upper
219 part of the convective cell is the lofting of condensate mass through the column by an underlying
220 updraft. The radial Doppler velocity (Fig. 1b) confirm the presence of an updraft (positive away
221 radial winds at the upper part of the cloud) within the 35 dBZ area. The flow divergence and
222 convective mass detrainment at the upper part of convective cell is nicely depicted by the
223 opposite sign radial Doppler velocity values. It is also plausible that the updraft vertical extent
224 reaches lower in the convective cell; however, the strongest changes in ΔZ are easier to detect
225 near the upper part of the cloud suggesting that the relationship between updraft strength and ΔZ
226 depends also on the background signal (Z_i).

227

228 More significant ΔZ changes throughout the storm are noted 94 s later by the time of the
229 third RHI at Δt_{94} (Fig. 1 e, f). Reflectivity changes in the core aloft (>10 km) are up to +20 dB
230 (0.2 dB s^{-1}), and the 35 dBZ (0 dBZ) echo top height has risen to 13 km (14.8 km),
231 corresponding to a change of 1000 m over 94 s, or an ascent rate of 10.6 m s^{-1} . On the other
232 hand, ΔZ in the mid-levels (4-6 km) are dominated by negative changes in reflectivity on the
233 order of -10 dB. Considering the rapid negative change in Z , we speculate that this could be
234 related to precipitation fall out of hail and rain or size sorting, and further studies supported by
235 model simulations will be required to better understand these processes and their relation to $\Delta Z /$
236 Δt . Similarly, almost 2 minutes later, (Δt_{113} Fig. 1 g, h), the increases in reflectivity aloft are > 20
237 dB, and decreases in the mid-levels exceed -20 dB. At lower levels (< 4 km), small decreases in
238 reflectivity are noted in the leading edge of the storm, whereas small positive changes on the
239 order of 3 dB are evident in the core (Fig. 1 g, h). In general, reflectivity changes in the anvil are
240 small ($< |5|$ dB), although the largest changes are on the underside of the anvils which could be
241 indicative of the anvil spreading out as well as stratiform fallout.

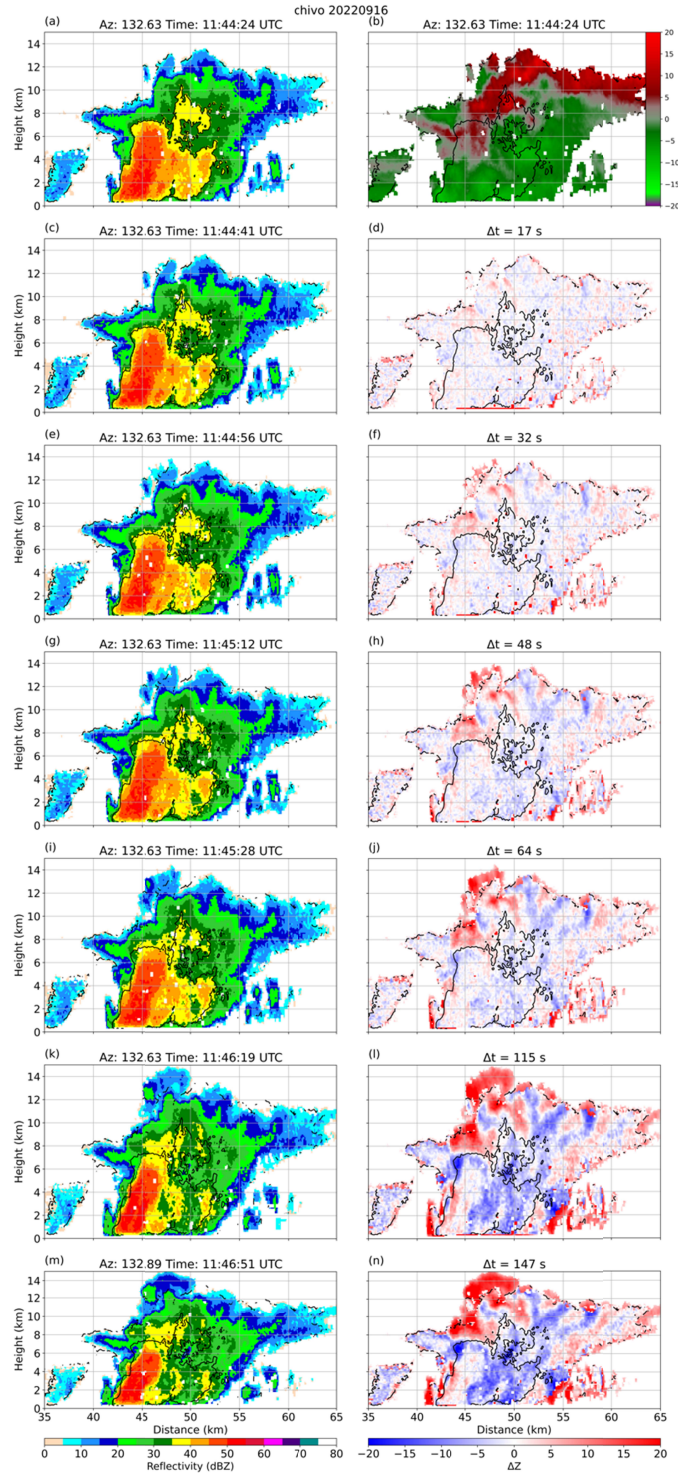
242
243
244

b. Case 2: The effect of temporal resolution on assessing convective storm evolution

245 The higher temporal resolution of the CHIVO radar is used here to investigate time resolved
246 radar reflectivity changes at even finer temporal resolutions than those proposed for the INCUS
247 mission. On 16 September 2022 at 11:44:24 UTC, MAAS targeted a convective cell at 45 km at
248 an azimuth of 132.63° from CHIVO. Case 2 features a much weaker convective core than Case
249 1, with a maximum reflectivity of 54 dBZ and 35 dBZ (0 dBZ) echo top height at t_0 of 10.4 km
250 (13.5 km, Fig. 3a). Local soundings (not shown) indicated significantly dry conditions in the
251 mid-levels that could be responsible for the weaker convective conditions. As in Case 1, the Case
252 2 isolated convective core is narrow, spanning less than 10 km in the horizontal (not shown). At
253 Δt_{17} , and similarly at Δt_{32} , changes in reflectivity are small ($< \pm 5$ dB) throughout the echo depth
254 (Fig. 3 c, d, 0.3 dB s^{-1}). However, some larger positive changes become apparent by Δt_{32} above
255 the intense core at 45 km range and at 8 km AGL (Fig. 3 e, f). During these Δt intervals, the 35
256 dBZ and 0 dBZ echo heights rise on the order of 100 m per 15 s to 10.8 km and 13.8 km,
257 respectively, after an interval of 32 s, corresponding to an ascent rate of the 35 dBZ echo top of
258 3.1 m s^{-1} . A more distinct pattern in ΔZ on the order of ± 5 dB is clear by Δt_{48} and Δt_{64} , with
259 positive changes to reflectivity above 8 km in the core, and some negative reflectivity changes at
260 farther distances (Fig. 3 g-j). At much longer time intervals (Δt_{115} and Δt_{147}), which are the next
261 available RHIs along this azimuth, the initial patterns of positive and negative ΔZ the same, with
262 larger magnitudes reaching +20 dBZ primarily in the upper levels of the storm, and -10 to -15
263 dBZ in the mid-level storm core and downrange of the convective core (Fig. 3 k-m). By the final
264 time Δt_{147} , the 35 dBZ echo height lowered to 10.1 km, but the 0 dBZ echo top height reached
265 15.2 km (Fig. 3 m, n).

266 In contrast to the more intense cell analyzed in Case 1, this case of relatively weak
267 convection generally had a reflectivity change less than 5 dB over a Δt of 32 s, while more
268 distinct regions of growth and decay became obvious by Δt_{48} with $\Delta Z > 5$ dB. In both cases,
269 growth of the convective core to higher altitudes was revealed through positive changes in
270 reflectivity, with ascent rates of the 35 dBZ echo top height on the order of 10 m s^{-1} in the
271 intense case 1 and 3.1 m s^{-1} in the weaker Case 2. These two high temporal resolution examples

272 demonstrate that weak and intense convection exhibit reflectivity changes of ~ 5 dB on time
 273 scales of 30 s or less, that growing parts



274
 275 Fig. 3: Case 2 investigation of temporal resolution on observing convective evolution.
 276 Timeseries of RHIs from the CHIVO radar on 16 September 2022 beginning at 11:44:24 UTC
 277 along the azimuth 123.6°. Reflectivity is shown at each time in the left panels, and reflectivity

278 differences from t_0 (a) are shown in the right panels. For reference the associated radial velocity
279 at t_0 is shown in (b).
280

281 of the storm (inferred from rising 35 dBZ echo heights) are associated with positive changes to
282 reflectivity in the mid- to upper-levels, and that the observed largest changes on these time scales
283 are in the upper portions of the storm where large regions of mass flux are expected as the
284 updraft lofts water and ice higher in the atmosphere.

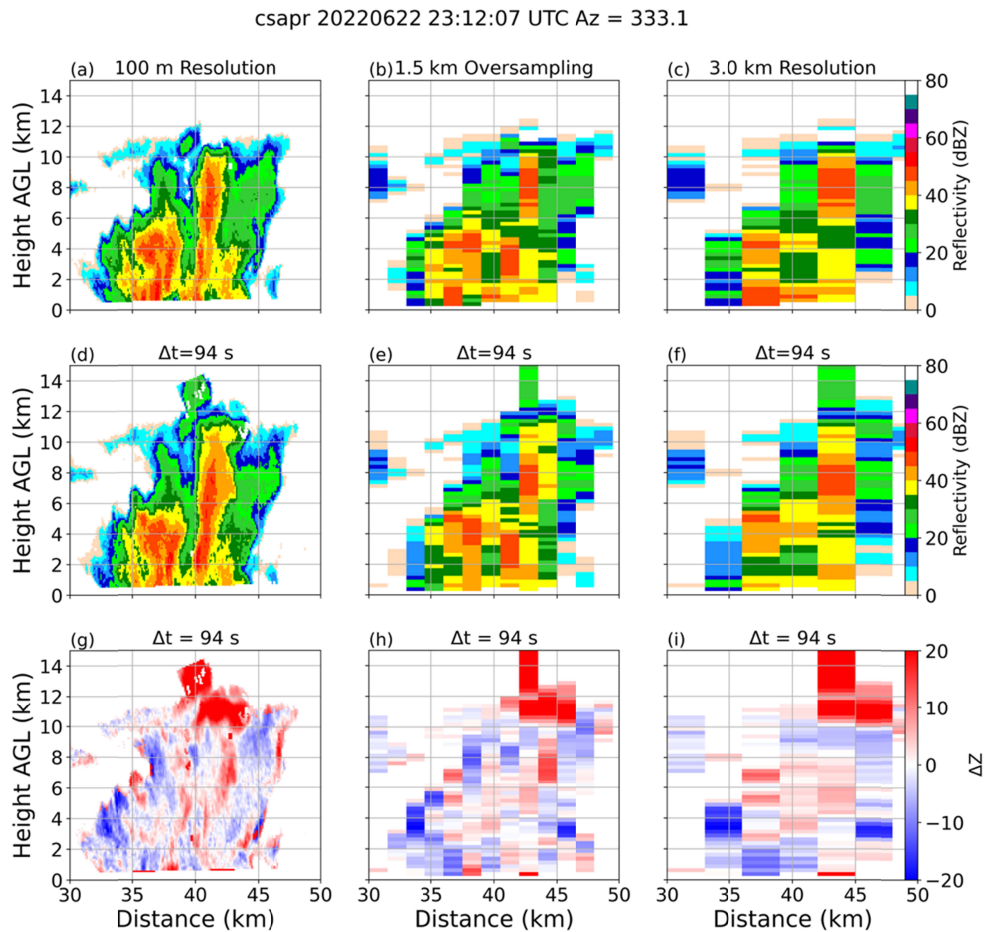
285
286

287 **c. Case 3: The effect of spatial resolution on assessing convective storm evolution**

288

289 The previous two cases highlighted that changes in reflectivity at high spatial resolution
290 (100 m) were notable even at time scales of 30 s or less. However, the ΔZ were estimated at high
291 spatiotemporal resolution. The INCUS radar constellation is expected to have Δt s like those
292 provided by the surface-based C-band radars, however the spatial resolution of the INCUS radars
293 is much coarser. Here, we investigate the impact of the INCUS radar footprint (~ 3 km) using an
294 example from CSAPR2 at 23:12:07 UTC on 22 June 2022 (Case 3, Fig. 4). Case 3 features two
295 convective cores, one with a 35 dBZ echo top height around 6.5 km, and a second, narrow
296 convective core, 3km wide, with 35 dBZ extending to 10 km (Fig. 4 a, d, g). The original, high-
297 resolution observations are horizontally smoothed using the 3 km long boxcar filter to represent
298 the INCUS antenna weighting function and vertically using a 0.25 km boxcar filter. The
299 smoothed radar reflectivity field is provided in two along track resolution at 1.5 km and 3.0 km
300 (Fig. 4 b,e,h and Fig. 4 c,f,i respectively). The 1.5 km along track integration represents a factor
301 of 2 oversampling sampling (Nyquist sampling, Sy et al., 2022) of the INCUS radar footprint, as
302 selected by the INCUS mission. The 3.0 km along track resolution is shown here for comparison.
303 Longer integration length along track is desirable for increasing the radar sensitivity, however, it
304 comes at the expense of smearing important convective cell features (Kollias et al., 2022a).
305 Overall, both the 1.5 km oversampled satellite (Fig. 4 b, e, h) footprint and the 3.0 km resolution
306 (Fig. 4 c, f, i) capture the general characteristics of these cores. In looking at the changes over
307 Δt_{92} , all resolutions show large increases in reflectivity (>20 dBZ) above 10 km as the convective
308 core at 43 km range grows. Similarly, positive ΔZ values are evident in the mid-levels (6 – 9 km
309 ASL), with a stronger column of positive changes in reflectivity $> \sim 10$ dB notable in the 100 m

310 resolution with the width of ~ 150 m, which is also evident in the 1.5 km oversampled satellite
 311 footprint. However, this same column of positive change is missed by the 3.0 km resolution
 312 observations. This suggests that 3.0 km may be too coarse to resolve changes to convection on
 313 small spatial scales even over longer temporal intervals. Finally, all resolutions indicate that the
 314 shallower convective core at 38 km away from the radar is decaying, with large negative ΔZ or
 315 small changes to the reflectivity in the core ($< \pm 5$ dB).
 316



317
 318 Fig. 4: Case 3 exploration of spatial resolution on observing convective evolution. CSAPR2
 319 RHIs from 22 June 2022 at 23:12:07 UTC along the azimuth of 333.1° (top row) and 94 s later
 320 (middle row) and the difference in reflectivity (bottom row) at 100 m resolution (left column),
 321 1.5 km oversampling and 250 m vertical resolution (middle column) and 3.0 km horizontal and
 322 250 m vertical resolution (right column).
 323

324 4. Discussion

325

326 The implementation of the MAAS framework in the recently conducted TRACER and
327 ESCAPE field campaigns around Houston TX, allowed us to collect high spatiotemporal
328 resolution observations in isolated convective cells, using traditional large-reflector radars. These
329 observations are ideal for a first evaluation of the NASA INCUS novel Δt measurement concept
330 using real observations.

331 The analysis of three isolated convective cells indicated that reflectivity differences on the
332 order of ~ 5 dB are observed over time scales of 20 s, underpinning the convective dynamics
333 driving the movement of water and air in the atmosphere. Changes of up to ~ 20 dB were evident
334 at longer timescales of more than one minute in all three cases. This finding suggests that the
335 INCUS mission selected Δt 's are appropriate for capturing small and large ΔZ signals. For
336 example, Case 2, an example of weaker convection illustrated changes of 10 dB were achieved
337 within 60 s and changes larger than 20 dB at time intervals longer than 90 s. Ascent rates of the
338 35 dBZ reflectivity contour were 10 m s^{-1} in a rapidly growing convective core (Case 1), and
339 were $\sim 3 \text{ ms}^{-1}$ in weaker isolated convection (Case 2). These results characterize the relationship
340 between changes in reflectivity and the underlying updraft which is moving water and air upward
341 in the atmosphere. The resulting ΔZ field contains coherent structures, a plausible indicators of
342 large coherent convective scale updrafts being the possible mechanism for their presence.

343 In addition, the observations verify that the INCUS radar footprint (~ 3 km) is not expected
344 to have a significant impact on determining the CMF and that the overall structure of convective
345 cells as depicted by the radar reflectivity is well computed. This is particularly true when we
346 oversampled by a factor of 2 the INCUS radar footprint, which is what is expected will be done
347 in the INCUS mission. In a nutshell, the INCUS radar sampling strategy is appropriate for
348 temporal and spatial sampling of convective cores. This said, some convective elements that
349 were smaller than the spatial resolution being considered were not resolved, even over longer
350 time scales of 94 s. Herein we have not directly related the observed changes in reflectivity to the
351 updraft strength from independent measurements of vertical velocity (such as from multi-
352 Doppler techniques). A separate manuscript that focuses on a more detailed verification of the
353 relationship between the observed ΔZ and the vertical air motion is under preparation.

354 The results presented here demonstrate the utility of using time differencing to understand
355 the scales of convective dynamics, both temporally and spatially. The findings herein will help to
356 guide future studies of convective dynamics, and our understanding of how best to utilize new

357 and advancing observational platforms with the ability to collect data at high temporal and
358 spatial resolutions. Future work is needed to examine if high resolution cloud resolving models
359 can accurately capture the storm dynamical processes observed using these types of rapidly-
360 scanned data. The role of advection and cloud microphysics in observed changes in reflectivity
361 over short time and horizontal scales also needs to be assessed.

362

363 **Acknowledgement:**

364

365 This work is supported by INCUS, a NASA Earth Venture Mission, funded by NASA's
366 Science Mission Directorate and managed through the Earth System Science Pathfinder Program
367 Office under contract number 80LARC22DA011. The authors extend appreciation to the entire
368 INCUS team for insightful discussions related to this work. Mariko Oue and Susan C. van den
369 Heever were also supported by Atmospheric System Research (grant no. DESC0021160).
370 Kristen Rasmussen was also supported by Atmospheric System Research (grant no. DE-
371 SC0022056). Mariko Oue and Pavlos Kollias were also supported by National Science
372 Foundation grant FAIN-2019932. Edward Luke and Katia Lamer were supported by the U.S.
373 Department of Energy, Atmospheric System Research (contract: DE-SC0012704).

374

375 **Open Research**

376

377 **Data Availability Statement:**

378

379 The CSAPR2 radar data used in this manuscript are available through the DOE ARM
380 archive (Oue et al., 2023) and the CHVIO radar data are available at the National Center for
381 Atmospheric Research Earth Observations Laboratory ESCAPE data archive
382 (https://www.eol.ucar.edu/field_projects/escape). Gridding was done with Radx2Grid
383 through LROSE (Bell et al. 2022). Figure 2 and some processing utilized the DOE-PyART
384 software (Helmus and Collis, 2016). Processing code including Radx parameter files and
385 plotting code is available from Dolan (2023).

386

387

388 **References:**

389

390 Bell, M. M., M. Dixon, W.-C. Lee, B. Javornik, J.DeHart, T.-Y. Cha, and A. DesRosiers, 2022:

391 nsf-irose/irose-topaz: irose-topaz stable final release 20220222 (irose-topaz-2022022).

392 [Software] Zenodo. <https://doi.org/10.5281/zenodo.6909479>

393 Bluestein, H. B., M. M. French, I. PopStefanija, R. T. Bluth, and J. B. Knorr, 2010: A mobile

394 phased-array Doppler radar for the study of severe convective storms. *Bull. Amer.*

395 *Meteor. Soc.*, 91, 579-600. <https://doi.org/10.1175/2009BAMS2914.1>

396 Bluestein, H. B., K. J. Thiem, J. C. Snyder , and J. B. Houser, 2019: Tornadogenesis and early

397 tornado evolution in the El Reno, Oklahoma, supercell on 31 May 2013. *Mon. Wea.*

398 *Rev.*, 147, 2045–2066, <https://doi.org/10.1175/MWR-D-18-0338.1>.

399 Brogniez H, Roca R, Auguste F, Chaboureau J-P, Haddad Z, Munchak SJ, Li X, Bouniol D,

400 Dépée A, Fiolleau T and Kollias P, 2022: Time-Delayed Tandem Microwave

401 Observations of Tropical Deep Convection: Overview of the C²OMODO Mission. *Front.*

402 *Remote Sens.* 3:854735. Doi: 10.3389/frsen.2022.854735

403 Crum, T. D., Saffle, R. E., and Wilson, J. W., 1998: An update on the NEXRAD program and

404 future WSR-88D support to operations. *Wea. For.*, 13(2), 253-262.

405 Dolan, B., 2023: GRL_dZdT [Software] Zenodo DOI: 10.5281/zenodo.8190935.

406 Fridlind, A.M., X. Li, D. Wu, M. van Lier-Walqui, A.S. Ackerman, W.-K. Tao, G.M.

407 McFarquhar, W. Wu, X. Dong, J. Wang, A. Ryzhkov, P. Zhang, M.R. Poellot, A.

408 Neumann, and J.M. Tomlinson, 2017: Derivation of aerosol profiles for MC3E

409 convection studies and use in simulations of the 20 May squall line case. *Atmos. Chem.*

410 *Phys.*, 17, 5947-5972, doi:10.5194/acp-17-5947-2017.

411 Griffith, P., Gunshor, M. M., Daniels, J. M., Goodman, S. J., and Lehair, W. J., 2017: A closer

412 look at the ABI on the GOES-R series. *Bull. Amer. Meteor. Soc.*, 98, 681-698.

413 Illingworth, A.J., Barker, H.W., Beljaars, A., Ceccaldi, M., Chepfer, H., Clerbaux, N., Cole, J.,

414 Delanoë, J., Domenech, C., Donovan, D.P. and Fukuda, S., 2015: The EarthCARE

415 satellite: The next step forward in global measurements of clouds, aerosols, precipitation,

416 and radiation. *Bull. Amer. Meteor. Soc.*, 96(8), pp.1311-1332.

417 Hartmann, D.L., H.H. Hendon and R.A. Houze, Jr., 1984: Some implications of the mesoscale

418 circulations in cloud clusters for large-scale dynamics and climate, *J. Atmos. Sci.*, 41,

419 113-121, 1984

420 Helmus, J.J. and Collis, S.M., 2016. The Python ARM Radar Toolkit (Py-ART), a Library for
421 Working with Weather Radar Data in the Python Programming Language. [Software] *J.*
422 *Open Res. Software*, 4(1), p.e25. DOI: <http://doi.org/10.5334/jors.119>

423 Jensen, M., and Coauthors, 2022: A succession of cloud, precipitation, aerosol and air quality
424 field experiments in the coastal urban environment. *Bull. Amer. Soc.*, **103**, 103-105.
425 <https://doi.org/10.1175/BAMS-D-21-0104.1>.

426 Kollias, P., N. Bharadwaj, E. Clothiaux, K. Lamer, M. Oue, J. Hardin, B. Isom, I. Lindenmaier,
427 A. Matthews, and E. Luke, 2020: The ARM Radar Network: At the leading edge of cloud
428 and precipitation observations, *Bull. Amer. Meteor. Soc.*, 1307 **101**(5), E588-E607.

429 Kollias P, Battaglia A, Lamer K, Treserras BP and Braun SA, 2022a: Mind the Gap - Part 3:
430 Doppler Velocity Measurements from Space. *Front. Remote Sens.* 3:860284. doi:
431 [10.3389/frsen.2022.860284](https://doi.org/10.3389/frsen.2022.860284)

432 Kollias, P., and Coauthors, 2022b: Science applications of Phased Array radars. *Bull. Amer.*
433 *Meteor. Soc.*, **103** (10), E2370-E2390. <https://doi.org/10.1175/BAMS-D-21-0173.1>

434 Lamer, K., P. Kollias, E. P. Luke, B. P. Treserras, M. Oue, and B. Dolan, 2023: Multisensor
435 Agile Adaptive Sampling (MAAS): a methodology to collect radar observations of
436 convective cell life cycle. *J. Atmos. Ocean. Technol.* Conditionally accepted.

437 Marinescu, P. J., P. C. Kennedy, M. M. Bell, A. J. Drager, L. D. Grant, S. W. Freeman, and S. C.
438 van den Heever, 2020: Updraft Vertical Velocity Observations and Uncertainties in High
439 Plains Supercells Using Radiosondes and Radars. *Mon. Wea. Rev.*, **148**, 4435-4452.
440 <https://doi.org/10.1175/MWR-D-20-0071.1>.

441 Oue, M., P. Kollias, A. Shapiro, A. Tatarevic, and T. Matsui, 2019: Investigation of
442 observational error sources in multi-Doppler-radar three-dimensional variational vertical
443 air motion retrievals, *Atmos. Meas. Tech.*, 12, 1999-2018, [https://doi.org/10.5194/amt-](https://doi.org/10.5194/amt-12-1999-2019)
444 [12-1999-2019](https://doi.org/10.5194/amt-12-1999-2019).

445 Oue, M., Saleeby, S. M., Marinescu, P. J., Kollias, P., and van den Heever, S. C., 2022:
446 Optimizing radar scan strategies for tracking isolated deep convection using observing
447 system simulation experiments, *Atmos. Meas. Tech.*, **15**, 4931–4950,
448 <https://doi.org/10.5194/amt-15-4931-2022>.

449 Oue, M., Treserras, BP., Luke, E., and Kollias, P., 2023: *CSAPR2 cell-tracking data collected*
450 *during TRACER*. [Dataset] United States: N. p. Web. doi:10.5439/1969992.

451 Palmer, R., and Coauthors, 2022: A primer on phased array radar technology for the atmospheric
452 sciences. *Bull. Amer. Meteor. Soc.*, **103**, E2205–2230, [https://doi.org/10.1175/BAMS-D-](https://doi.org/10.1175/BAMS-D-21-0172.1)
453 [21-0172.1](https://doi.org/10.1175/BAMS-D-21-0172.1).

454 Peral, E., and Coauthors, 2019: RainCube: The first ever radar measurements from a CubeSat in
455 space. *J. Appl. Remote Sens.*, **13**, 032504, <https://doi.org/10.1117/1.JRS.13.032504>.

456 Pazmany, A. L., J. B. Mead, H. B. Bluestein, J. C. Snyder, and J. B. Houser, 2013: A mobile,
457 rapid-scanning, X-band, polarimetric (RaXPoL) Doppler radar system. *J. Atmos. Oceanic*
458 *Technol.*, **30**, 1398–1413, <https://doi.org/10.1175/JTECH-D-12-00166.1>.

459 Sherwood, S. C., S. Bony and J.-L. Dufresne, 2014: Spread in model climate sensitivity traced to
460 atmospheric convective mixing. *Nature*, 505, 37-42. Doi:10.1038/nature12829

461 Stephens G., Freeman A., Richard E., Pilewskie P., Larkin P., Chew C., Tanelli S., Brown S.,
462 Posselt D., Peral E., 2020a: The emerging technological revolution in Earth
463 observations. *Bull. Amer. Meteor. Soc.* 101, E274–E285

464 Stephens G., and Coauthors, 2020b: A Distributed Small Satellite Approach for Measuring
465 Convective Transports in the Earth’s Atmosphere, *IEEE Trans. Geo. Remote Sens.*, **58**
466 (1), 4-13, doi: 10.1109/TGRS.2019.2918090

467 Su, H., Jiang, J. H., Zhai, C., Shen, T. J., Neelin, J. D., Stephens, G. L., & Yung, Y. L., 2014:
468 Weakening and strengthening structures in the Hadley Circulation change under global
469 warming and implications for cloud response and climate sensitivity. *J. Geophys. Res.: Atmos.*, **119**(10), 5787-5805.

471 Sy. O. O., and Coauthors, 2022: Scientific Products from the First Radar in a CubeSat
472 (RainCube): Deconvolution, Cross-Validation, and Retrievals. *IEEE Trans. Geo. Remote*
473 *Sens.*, **60**, 1-20, doi: 10.1109/TGRS.2021.3073990.

474 Tanamachi, R. L., and P. L. Heinselman, 2016: Rapid-scan, polarimetric observations of
475 central Oklahoma severe storms on 31 May 2013. *Wea. Forecasting*, 31,19–42,
476 <https://doi.org/10.1175/WAF-D-15-0111.1>.

477 Wehr, T., Kubota, T., Tzeremes, G., Wallace, K., Nakatsuka, H., Ohno, Y., Koopman, R., Rusli,
478 S., Kikuchi, M., Eisinger, M. and Tanaka, T., 2023. The EarthCARE Mission–Science
479 and System Overview. *EGUsphere*, pp.1-47.

480 van den Heever, 2021: NASA Selects New Mission to Study Storms, Impacts on Climate
481 Models, *NASA Earth*. [https://www.nasa.gov/press-release/nasa-selects-new-mission-to-](https://www.nasa.gov/press-release/nasa-selects-new-mission-to-study-storms-impacts-on-climate-models)
482 [study-storms-impacts-on-climate-models](https://www.nasa.gov/press-release/nasa-selects-new-mission-to-study-storms-impacts-on-climate-models).

483